Journal of Alloys and Compounds 509 (2011) 7071–7077

Contents lists available at ScienceDirect

Journal of Alloys and Compounds

journal homepage: www.elsevier.com/locate/jallcom

Combustion synthesis and characterization of highly crystalline single phase nickel ferrite nanoparticles

T. Prabhakaran, J. Hemalatha*

Advanced Materials Lab, Department of Physics, National Institute of Technology, Tiruchirappalli 620 015, Tamilnadu, India

ARTICLE INFO

Article history:
Received 3 December 2010
Received in revised form 23 March 2011
Accepted 30 March 2011
Available online 6 April 2011

Keywords:
Magnetically ordered materials
Chemical synthesis
Magnetization
X-ray diffraction
FTIR
Hysteresis

ABSTRACT

A combustion route of synthesizing highly crystalline single phase nickel ferrite ($NiFe_2O_4$) spinel nanoparticles using various amounts of DL-alanine as fuel has been reported in this paper. The role of the amount of fuel is found to be significant in the size control and phase purity of nano crystalline samples. The structural, thermal, morphological and magnetic studies have been carried out. XRD patterns reveal the formation of highly crystalline nano $NiFe_2O_4$ with high degree of phase purity when fuel concentration is maintained at 1 M and 2 M. FTIR spectra also prove the formation of pure nano $NiFe_2O_4$. The temperature and fuel effects are found to have strong influence on size, structural, and magnetic properties of materials. The magnetic measurements show that the nano $NiFe_2O_4$ samples exhibit soft ferromagnetism with the highest saturation magnetization Ms at room temperature as 42.53 emu/g.

1. Introduction

Synthesis of spinel ferrite nanomaterials has attracted a great deal of attraction over the past several years, due to their functional electrical and magnetic properties. These types of ferrites are widely used in the field of magnetic drug delivery, magnetic information storage device, ferrofluids, sensors, catalysis, etc. [1–6]. Among these spinel ferrites, the inverse type is more interesting due to its high magneto crystalline anisotropy and high saturation magnetization. Nickel ferrite ($NiFe_2O_4$) is one of the most important materials in the inverse spinel family exhibiting ferrimagnetic properties combined with relatively low electrical properties and it displays low eddy current loss in alternating current applications. Nickel ferrite unit cell contains 32 oxygen atoms in a cubic close packing with eight tetrahedral (A) and sixteen octahedral (B) sites. Half of the ferric ions preferentially fill the A-sites and the others occupy the B-sites. Thus the compound can be represented by the formula $(Fe^{3+})_A [Ni^{2+} Fe^{3+}]_B O_4^{2-}$ [7,8]. However, it shows ferrimagnetism that orginates from magnetic moment of antiparallel spins between Fe^{3+} ions at tetrahedral sites and Ni^{2+} ions at octahedral sites [9].

The preparation and characterization of $NiFe_2O_4$ in nanoscale would allow investigating the fundamental aspects of anomalous properties different from those of bulk properties. There are plenty of methods available to synthesize $NiFe_2O_4$ nanostructures including sol gel [10,11], hydrothermal [12–14], co-precipitation [7,15], RF – plasma torch method [16], chemical route [17], ball milling [18], combustion methods [7,8,14,18–23]. However, developing synthetic approaches to prepare nickel ferrite nanoparticles with controlled size and morphology seem to be a highly sophisticated challenge to materials scientists and chemists [24].

In particular, the synthesis by combustion reaction technique has been shown to have great potential in the preparation of ferrites. This process is quite simple and involves an exothermic and self-sustaining chemical reaction between the metal salts and a suitable organic fuel, usually urea [22], glycine [8], hydrazides [25], citric acid [19–21,23].

To the best of our knowledge no attempt was made earlier to use DL-alanine as fuel for synthesis of nano nickel ferrite. DL-Alanine is a common amino acid used as a reducing fuel to achieve synthesize of ferrites at low temperature. It belongs to the same amino acid series as glycine, but unlike glycine it has an extra branched methyl group that might cause evolution of a large quantity of gases during combustion resulting in fine particles [26]. After chelating process between divalent metal ions the combustion reaction occurs at low temperature and produce highly crystalline ferrite nanoparticles. This paper reports and discusses the synthesis of nano sized single phase crystalline nickel ferrite via combustion method by using DL-alanine as fuel. The results of investigations on the structural, thermal, topographical and magnetic studies of nano nickel ferrite samples prepared using various amounts of fuel are reported.

* Corresponding author. Tel.: +91 04312503608; fax: +91 04312500133.
E-mail address: hemalatha@nitt.edu (J. Hemalatha).

0925-8388/$ – see front matter © 2011 Elsevier B.V. All rights reserved.
doi:10.1016/j.jallcom.2011.03.176

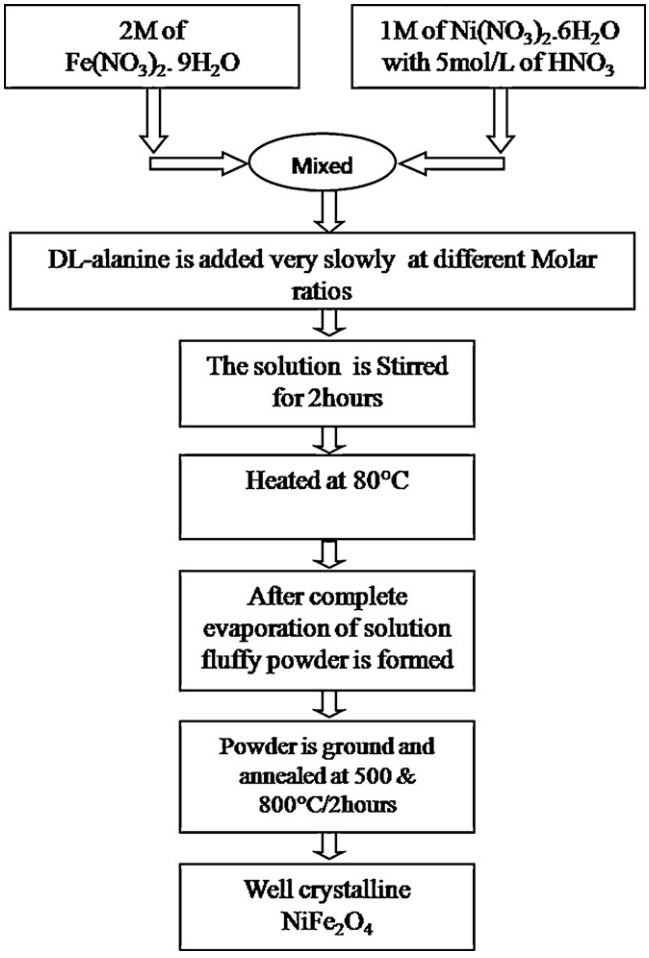

Fig. 1. Steps involved in synthesis.

2. Experimental

2.1. Synthesis

All the chemicals used in this reaction were of analytical grade and were used as purchased. Nickel nitrate Ni $(NO_3)_2{\cdot}6H_2O$ and iron nitrate Fe $(NO_3)_2{\cdot}9H_2O$ were used as the reactants. Double distilled water was used as solvent whereas DL-alanine ($C_3H_7NO_2$) was used as the fuel for combustion [24].

Aqueous solutions of nickel and ferric nitrates were prepared separately in stoichiometric ratio 1:2 to obtain cation precursors. 5 mol/L of nitric acid was added to the aqueous nickel nitrate solution and it was stirred manually. The mixture thus formed was added to the iron nitrate solution while stirring. Required quantities of aqueous DL-alanine solution were added to the solution mixture slowly after half an hour of vigorous stirring. The final solution was stirred for 2 h and heated at 80 °C to initiate self propagating exothermic reaction. While heating, the mixture started vaporizing with great deal of foams produced. Spark appeared in a corner which spread through the entire mass, yielding a voluminous and dark brown fluffy product in the container. The acquired substance was ground into a fine powder which is then annealed for 2 h at 500 °C and 800 °C, respectively. The synthesis process is illustrated in Fig. 1. Combustion was attempted with three different amounts of fuel because the amount of fuel controls the combustion temperature and time thereby has important effects on the characteristics of the final product. In this investigation the ratio of DL-alanine:nickel nitrate:ferric nitrate was kept as (1–3):1:2. Fig. 2 depicts the photographs taken at different stages of synthesis.

2.2. Characterization

The crystalline structure, phase composition and crystallite size of as-prepared and annealed NFO samples were identified from XRD patterns obtained using Cu Kα radiation (λ = 1.541 Å) for 2θ value ranges from 10° to 80° in X-ray diffractometer (Model Rigaku Ultima III). The Fourier transform Infrared (FTIR) transmission spectrum of the samples mixed with KBr powder reference were obtained from 1000 cm^{-1} to 400 cm^{-1} using Perkin Elmer spectrophotometer (Spectrum RX1). The thermal stability and weight loss of the samples were investigated through TGA (Model Perkin Elmer) in argon gas from 50 °C to 950 °C with a heating rate of 20 °C/min. Field emission scanning electron micrographs (FESEM) were recorded on Model Zeiss EVO 50. The size of nano particles were characterized using CM200 PHILIPHS transmission electron microscope (TEM). Sample for TEM analysis was prepared by drying a drop of $NiFe_2O_4$–ethylene glycol mixture on amorphous carbon-coated copper grid. The magnetic properties of samples were obtained at room temperature using a vibrating sample magnetometer (Lake Shore, USA, Model 7404) with 16.5 KOe as maximum applied magnetic field.

3. Results and discussion

3.1. Structural analysis

The XRD patterns of as-prepared and annealed samples obtained using different concentrations of DL-alanine are shown in Fig. 3. They exhibit typical reflections of (1 1 1), (2 2 0), (3 1 1), (2 2 2), (4 0 0), (4 2 2), (5 1 1), (4 4 0), (6 2 0) and (5 3 3) planes indicating the cubic spinel structure of nickel ferrite. All the peaks match well with the standard JCPDS 86-2267. The strong and sharp reflection peaks indicate the high crystallinity of the samples. In samples (S1–S3) prepared with 1 M of fuel, the crystallinity is enhanced remarkably after annealing at 800 °C. The samples (S4–S6) prepared with 2 M of fuel exhibit strong and sharp peaks. They are observed to be well crystallized irrespective of the heat treatments.

No secondary peaks are detected in XRD patterns of above mentioned samples (S1–S6) which ensure the phase purity of the samples. But the samples (S7–S9) prepared using 3 M of fuel show some secondary peaks corresponding to Fe_2O_3, β-Fe_2O_3 and Ni_2O_3. So, it is understood that impurity phases coexist with nano $NiFe_2O_4$ when the fuel concentration is increased to 3 M.

The average grain size is obtained using Debye Scherrer equation [27]

$$D = \frac{0.9\lambda}{\beta_{h\ k\ l}\cos\ \theta} \quad (1)$$

Where β_{hkl} is full width at half maximum of the diffraction peak, λ is wavelength of X-ray 1.541 Å and θ is Bragg angle.

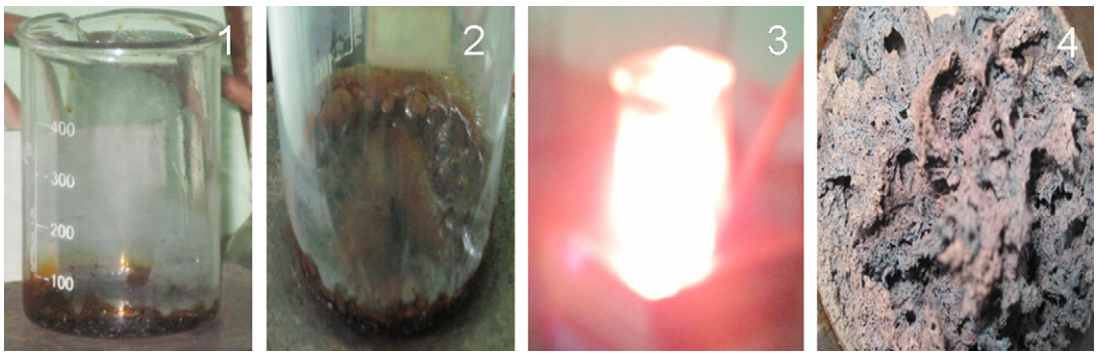

Fig. 2. (1) Precursor solution added with DL-alanine (2) foams produced during heating (3) combustion and (4) fluffy final product.

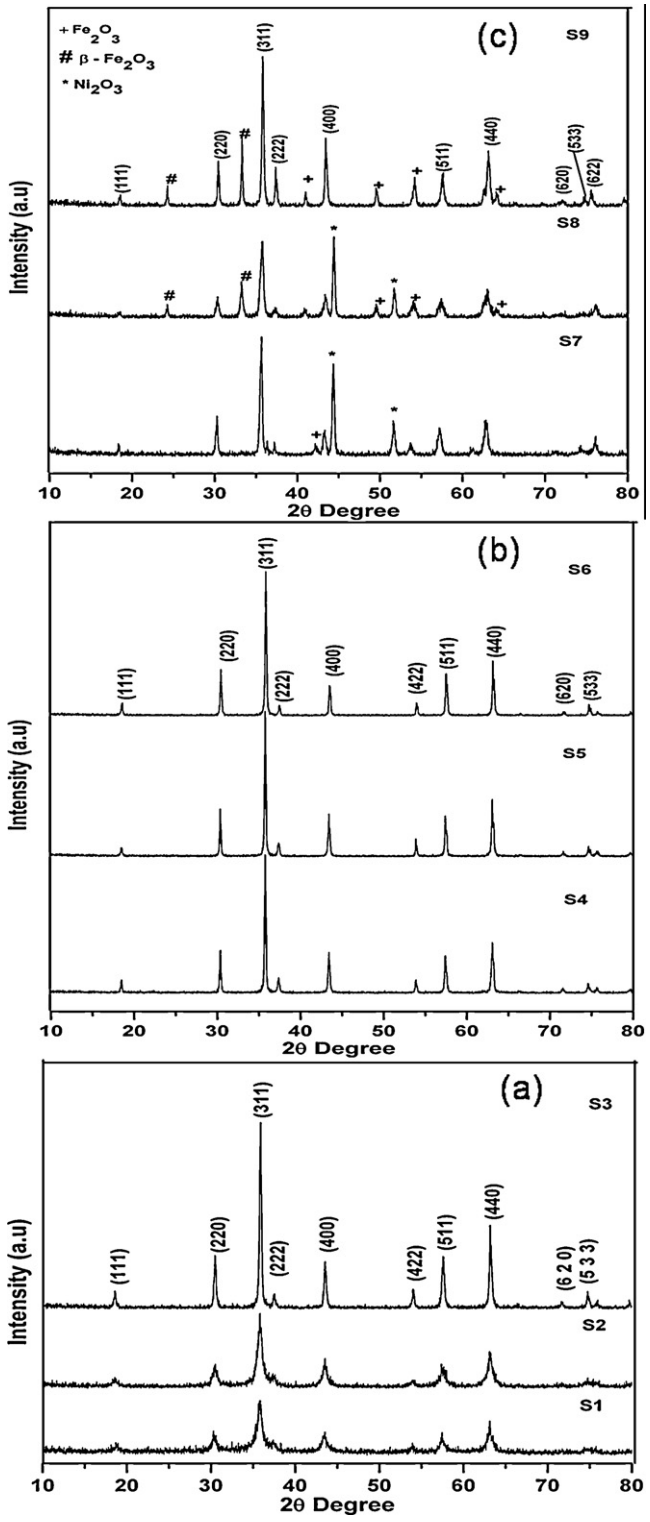

Fig. 3. XRD pattern of as-prepared, annealed at 500 °C and 800 °C samples prepared using (a) 1 M of DL-alanine, (b) 2 M of DL-alanine and (c) 3 M of DL-alanine.

The instrumental corrected broadening, (β_{hkl}) corresponding to each diffraction peak of nanocrystalline $NiFe_2O_4$ was estimated using the following relation [28].

$$(\beta_{h\ k\ l})^2 = (\beta_{h\ k\ l})^2 \text{ measured} - (\beta_{h\ k\ l})^2 \text{ instrumental} \quad (2)$$

The estimated values of crystallite sizes and lattice constants of all the samples (S1–S9) are listed in Table 1. It is seen from Fig. 3a that the peaks become narrower for sample S3 compared to S1 and S2, indicating the increase in crystallite size. The Debye Scherrer equation gives the increased crystallite size of 26 nm for sample S3 which was annealed at 800 °C.

Table 1
Sample code, lattice parameter and crystallite size of the samples.

Sample	Sample code	Lattice constant ($a = b = c$) (nm)	Size (nm)
1 M as-prepared	S1	0.832	12.32
500 °C/2 h	S2	0.831	11.90
800 °C/2 h	S3	0.830	26.00
2 M as-prepared	S4	0.833	34.50
500 °C/2 h	S5	0.833	35.30
800 °C/2 h	S6	0.831	35.00
3 M as-prepared	S7	0.836	23.30
500 °C/2 h	S8	0.834	18.80
800 °C/2 h	S9	0.831	26.40

There is no significant change in the sizes of samples S4–S6 which are as-prepared and thermally treated. Thus independent of the annealing temperature the size of samples prepared with 2 M solution of fuel is 35 nm. XRD patterns of S7–S9 reveal that more impurity peaks appear with increase of annealing temperature. The size of the crystallite has grown in size at higher annealed temperature.

The lattice constants of all the samples are calculated using the relation [29]

$$a = d_{k\ h\ l}\sqrt{h^2 + k^2 + l^2} \quad (3)$$

and are included in Table 1. The values are in good agreement with earlier reported values of 0.833 nm for nano $NiFe_2O_4$ [13] and 0.8339 nm for the bulk $NiFe_2O_4$ [30] which prove the efficiency of synthesis technique.

3.2. Morphology and composition analysis

The morphology of the nano $NiFe_2O_4$ samples investigated through FESEM is shown in Fig. 4. The particles are found agglomerated due to magnetic dipole interaction among the particles. The TEM (Fig. 5) of sample S6 shows the particles of size in the range of 20–45 nm.

The EDX spectra for the samples S4–S6 are shown in Fig. 4 and the composition details are listed in Table 2. It is obvious that the sample contains only O, Fe, and Ni and no other contamination elements. The atomic ratio of Ni to Fe is 1:2 which matches the exact stoichiometric ratio of nickel ferrite. The extra peak at 2.14 keV can be attributed to the sample grid of FESEM.

3.3. FTIR analysis

The infrared spectra obtained for S4 and S6 in the range 400–1000 cm^{-1} are shown in Fig. 6. The spectra show two main absorption bands around 600 and 400 cm^{-1}. Intrinsic stretching vibrations of metal at tetrahedral site, $M_{tetra} \leftrightarrow O$, υ_1, are generally observed in the range of 620–550 cm^{-1}. The stretching vibrations of metal at octahedral site, $M_{octa} \leftrightarrow O$, υ_2, are generally observed in the range 450–385 cm^{-1} [8,12,31,32]. In Fig. 6, $Fe \leftrightarrow O$, υ_1 stretching vibration observed at 550 and 586 cm^{-1} and $Ni \leftrightarrow O$, υ_2 stretching vibration observed at 457 and 411 cm^{-1} confirm the presence of spinel cubic $NiFe_2O_4$. The variations in the band positions of S4 and S6 are due to the difference in the Fe–O and Ni–O distances initiated by the redistribution of ions at higher temperature. Similar shift is reported by Balaji et al. [33] in NFO samples synthesized through combustion method where urea has been used as the fuel.

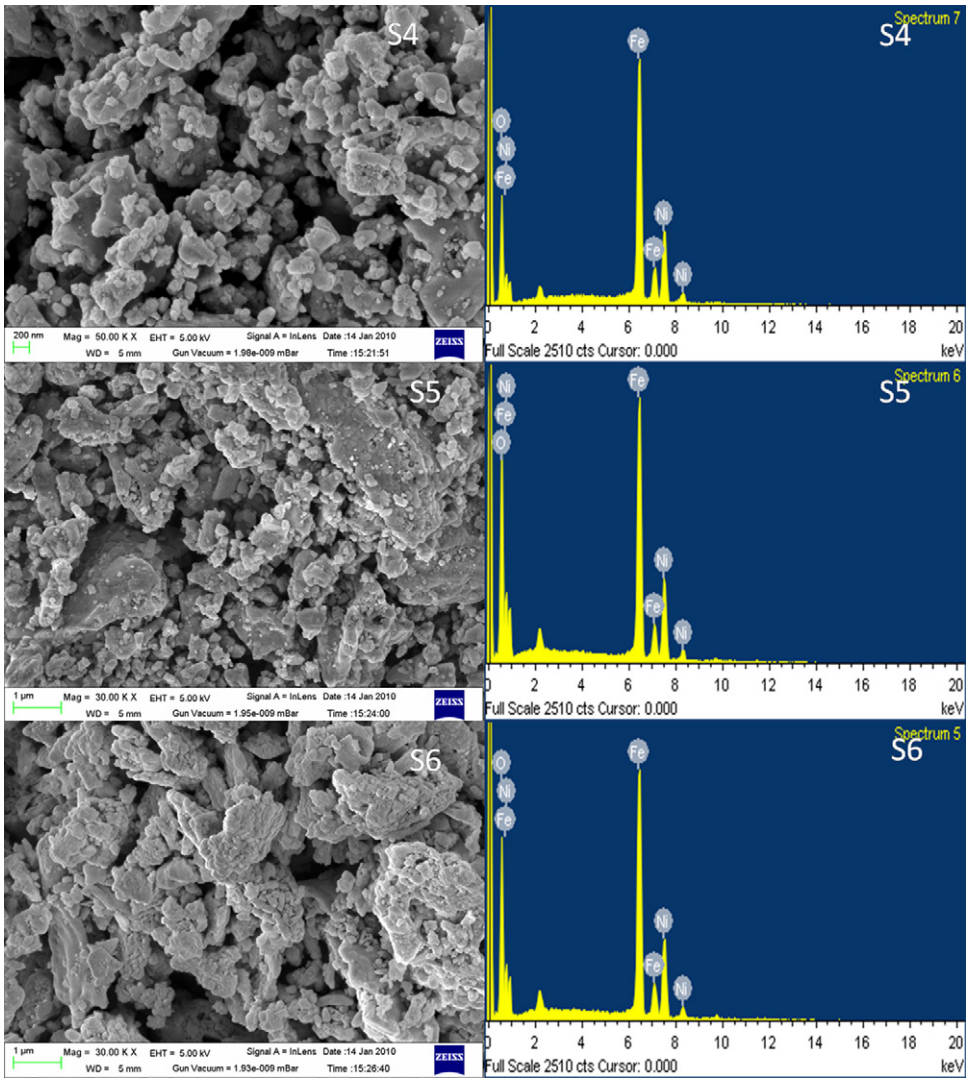

Fig. 4. FESEM images and EDX spectra recorded for samples S4–S6.

3.4. Thermal studies

Fig. 7 shows the TGA traces obtained for S4–S6. The traces obtained for as-prepared sample S4 exhibits the apparent fall from 350 °C to 380 °C which may be ascribed to the processes such as decomposition of residual DL-alanine, and nitrate groups. The samples S5 and S6 which are annealed at elevated temperatures do not show any fall due to decomposition in this region because they are already heat-treated at the temperature higher than the decomposition temperature. Moreover they show higher thermal stability up to 950 °C than S4.

3.5. Magnetic measurements

Room temperature magnetization studies made for $NiFe_2O_4$ samples S3, S6 and S9 are shown in Fig. 8. The inset is the magnified image which illustrates the shape of the loop. The magnetization behavior of the samples is of typical soft ferromagnets which can be explained on the basis of changes in exchange interaction between tetrahedral and octahedral sub-lattices. However in nano particles of ferrites there is interplay of four factors namely super-exchange interaction, magneto crystalline anisotropy, canting effect and dipolar interactions between the projected moments on the surface

Table 2
Stoichiometry composition from EDX.

Element	S4		S5		S6	
	Weight %	Atomic %	Weight %	Atomic %	Weight %	Atomic %
O K	15.95	40.23	26.12	55.64	22.63	50.94
Fe K	56.51	40.84	49.25	30.06	51.13	32.97
Ni K	27.54	18.93	24.63	14.30	26.24	16.09
Totals	100.00		100.00		100.00	

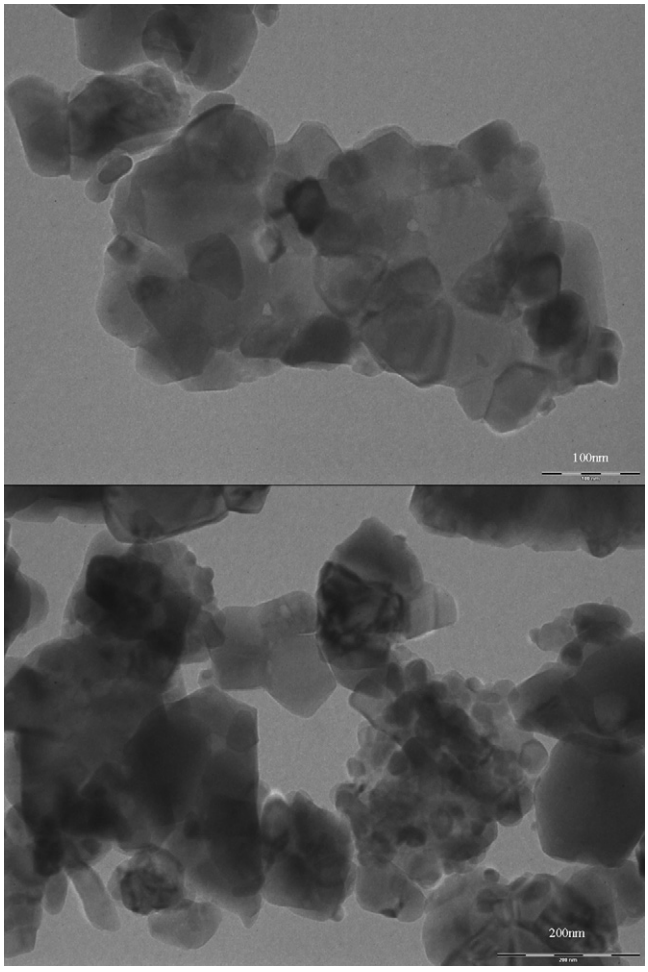

Fig. 5. TEM image of sample S6.

of nanoparticles. Hence the magnetic property observed in nano $NiFe_2O_4$ is a cumulative effect of these interactions [8,34–36].

Sample S6 with crystallite size 35 nm exhibits a saturation magnetization (Ms) of 42.5 emu/g which is higher than the values reported for room temperature [12,38]. But the value is lower than that for bulk $NiFe_2O_4$ reported as 55 emu/g in [37,38]. Ms of sample S3 having crystallite size of 26 nm is reduced to 39.8 emu/g. It

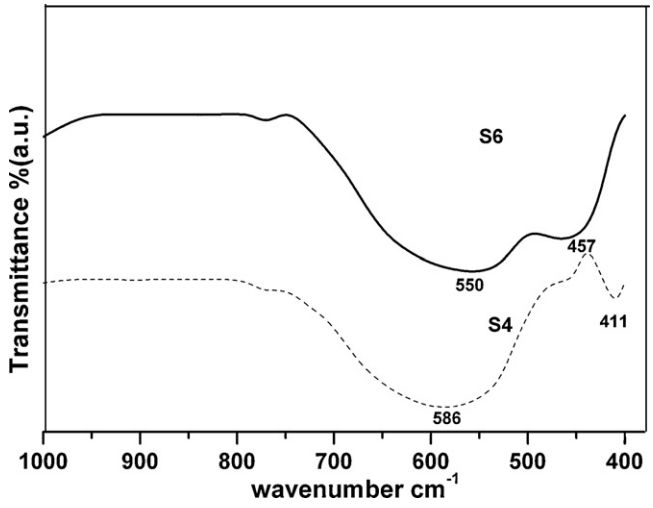

Fig. 6. FTIR spectra of nano $NiFe_2O_4$ samples.

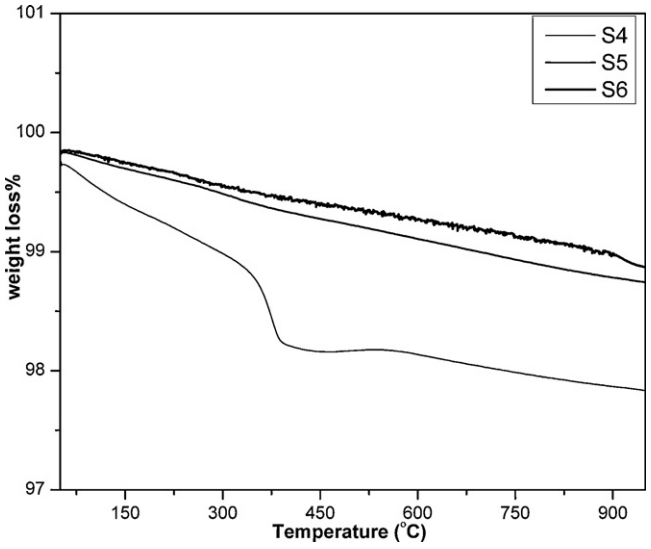

Fig. 7. TGA traces of nano $NiFe_2O_4$ samples.

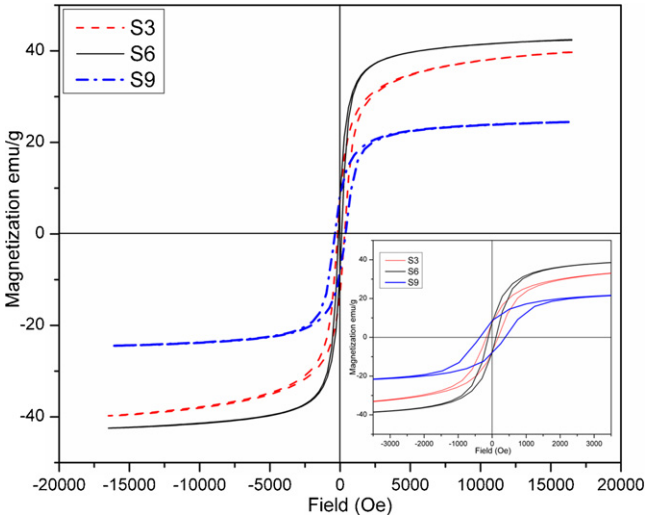

Fig. 8. Hysteresis plots obtained for nano $NiFe_2O_4$.

is well known that for magnetic nano particles the size has significant influence on their magnetic properties [39]. Moreover, better crystallinity of sample S6 contributes higher magnetization when compare to sample S3.

Sample S9 though has the same crystallite size of 26 nm as S3 shows still low value of Ms. The reason for this decrease is attributed to the impurity phases of Fe_2O_3 and Ni_2O_3 present in the sample which is evident from the XRD studies.

The Coercivity and retentivity values are also listed in Table 3. Compared with the H_c value of bulk $NiFe_2O_4$ reported in literature (close to 0 Oe) [38], nano $NiFe_2O_4$ exhibits larger coercivity which can be attributed to the nanostructure [40,41]. The coercivity of

Table 3
Size and magnetic values of $NiFe_2O_4$.

Sample	Size (nm)	Saturation magnetization Ms (emu/g)	Coercivity H_c (Oe)	Retentivity Mr (emu/g)
S3	26.0	39.774	172.29	7.3081
S6	35.0	42.500	112.35	7.9220
S9	26.4	24.449	372.01	8.1901

Table 4
Comparison of phase purity and saturation magnetization of our sample with those reported earlier.

S. no	Preparation method	Grain size (nm)	Phase purity	Saturation magnetization Ms (emu/g)
1	Combustion using DL-alanine as a fuel (present work)	35.00 at 800 °C/2 h	Pure	42.500
2	Sol gel auto combustion CTAB used as cationic surfactant [19]	61.4, 31.2 for 1000 °C	Fe_2O_3 is present pure only above 1000 °C	–
3	Sol gel auto combustion [20] citric acid as fuel	72 at 1000 °C	Fe_2O_3 is present pure only above 1000 °C	54
4	Hydrothermal [41]	10–35	Pure	30.4
5	Hydrothermal [42]	39	Pure	0.00015
6	Co precipitation [43]	14 28 32	Pure	41.5 36.1 45.8
7	Co precipitation [44]	30–100	Impure phases $Fe_2O_3{\cdot}H_2O$ and FeO(OH) observed at 800 °C	32.0 for 1000 °C, 2.7 for 500 °C
8	Solid state reaction [45]	32.4	Pure	35.00
9	Sonochemical method [38]	Size is less than 25 nm	Pure	25

S9 is significantly high when compared to other two values which may be attributed to the presence of impurity in that sample. Coercivity values of pure phase S3 and S6 samples show a decreasing trend as the particle size decreases. Also, due to lower crystallinity and smaller size the porosity of S3 would be higher and hence the coercivity of S3 is higher than that of S6. The variation of H_c with particle size can be explained on the basis of domain structure, critical diameter and anisotropy of the crystal [8,17,34–36].

Table 4 illustrates a comparison of the grain size, phase purity and saturation magnetization of our NFO sample (S6) with those reported earlier. Perusal of the table gives an idea that the samples synthesized through other methods and also through same combustion method but with different fuels, lack either in phase purity or in the saturation magnetization. However, the properties of our sample appear to be comparable with those reported by Umare et al. [43] which were arrived through co precipitation method with ethylene glycol as solvent and capping agent.

4. Conclusion

In summary, nano sized $NiFe_2O_4$ has been prepared through combustion route by using DL-alanine as fuel. According to the XRD spectra, the samples prepared with 2 M of fuel have better crystallinity than those prepared with 1 M of fuel, where the samples prepared with 3 M fuel showed the appearance of secondary peaks. Therefore, 2 M of fuel is preferable to prepare single phase $NiFe_2O_4$ nanoparticles with better crystallinity. FTIR and EDX studies also confirm the formation of impurity free nano $NiFe_2O_4$. A FESEM study shows the agglomerated particles. The particle size distribution estimated from XRD is in good agreement with that estimated through TEM. The room temperature VSM studies show that the nano $NiFe_2O_4$ particles exhibit soft ferromagnetic nature with high saturation magnetization of 42.4 emu/g. So it can have potential applications in soft magnets, ferrofluids and low loss materials at high frequencies, drug delivery and magnetic resonance imaging.

Acknowledgment

We thank Dr. Justin Joseyphus and Dr. S. Kumaran, Assistant Professors, NITT for extending the instrumentation facility for characterization. The authors acknowledge the DST, Government of India for the VSM facility under the FIST programme sanctioned to Department of Physics, NIT, Tiruchirappalli.

References

[1] J. Zhang, J. Shi, M. Gong, J. Solid State Chem. 182 (8) (2009) 2135–2140.
[2] I. Safarik, M. Safarikova, Nanostructured Materials, Springer, Vienna, 2002, pp. 1–23.
[3] M.P. Pileni, Adv. Funct. Mater. 5 (2001) 323–333.
[4] F.Y. Cheng, C.H. Su, Y.S. Yang, C.S. Yeh, C.Y. Tsai, C.L. Wu, M.T. Wu, D.B. Shieh, Biomaterials 26 (2005) 729–738.
[5] Q. Song, Z.J. Zhang, J. Am. Chem. Soc. 126 (2004) 6164–6168.
[6] J. Sun, S. Zhou, P. Hou, Y. Yang, J. Weng, X. Li, M. Li, J. Biomed. Mater. Res. A 80A (2007) 333–341.
[7] M. Salavati-Niasari, F. Davar, T. Mahmoudi, Polyhedron 28 (2009) 1455–1458.
[8] A. Alarifi, N.M. Deraz, S. Shaban, J. Alloys Compd. 486 (2009) 501–506.
[9] Y. Kinemuchi, K. Ishizaka, H. Suematsu, W. Jiang, K. Yatsui, Thin Solid Films 407 (2002) 109–113.
[10] M. Srivastava, A.K. Ojha, S. Chaubey, A. Materny, J. Alloys Compd. 481 (2009) 515–519.
[11] D.-H. Chen, X.-R. He, Mater. Res. Bull. 36 (2001) 1369–1377.
[12] Y. Cheng, Y. Zheng, Y. Wang, F. Bao, Y. Qin, J. Solid State Chem. 178 (2005) 2394–2397.
[13] J. Huo, M. Wei, Mater. Lett. 63 (2009) 1183–1184.
[14] H. Kavas, N. Kasapoglu, A. Baykal, Y. Koseoglu, Chem. Pap. 63 (2009) 450–455.
[15] X. Cao, L. Gu, Nanotechnology 16 (2005) 180–185.
[16] S. Son, M. Taheri, E. Carpenter, V.G. Harris, M.E. McHenry, J. Appl. Phys. 91 (2002) 7589–7591.
[17] S. Maensiri, C. Masingboon, B. Boonchom, Supapan, Scripta Mater. 56 (2007) 797–800.
[18] J.H. Liu, L. Wang, F.S. Li, J. Mater. Sci. 40 (2005) 2573–2575.
[19] M.R. Barati, S.A. Seyyed Ebrahimi, A. Badiei, J. Non-Cryst. Solids 354 (2008) 5184–5185.
[20] J. Azadmanjiri, S.A. Seyyed Ebrahimi, H.K. Salehani, Ceram. Int. 33 (2007) 1623–1625.
[21] A. Pradeep, P. Priyadharsini, G. Chandrasekaran, Mater. Chem. Phys. 112 (2008) 572–576.
[22] M.A.F. Ramalho, L. Gama, S.G. Antonio, C.O. Paiva-Santos, E.J. Miola, R.H.G.A. kiminami, A.C.F.M. Costa, J. Mater. Sci. 42 (2007) 3603–3606.
[23] A.T. Raghavender, Kreso Zadro, Damir Pajic, Zeljko Skoko, Nikola Billiškov, Mater. Lett. 64 (2010) 1144–1146.
[24] J. Wang, F. Ren, Yi Ran, A. Yan, G. Qiu, X. Liu, J. Alloys Compd. 479 (2009) 791–796.
[25] Y.K. Sun, I.H. Oh, S.A. Hong, J. Mater. Sci. 31 (1996) 3617–3621.
[26] M.W. Raja, S. Mahanty, P. Ghosh, R.N. Basu, H.S. Maiti, Mater. Res. Bull. 42 (2007) 1499–1506.
[27] H.P. Klug, L.E. Alexander, X-ray Diffraction Procedure, Wiley Inter Science, New York, 1954, pp. 504.
[28] V. Biju, N. Sugathan, V. Vrinda, S.L. Salini, J. Mater. Sci. 43 (2008) 1175–1179.
[29] B.D. Cullity, Elements of X-ray diffraction, Addision Wesley Pub. Co. Inc., 1956, p. 42.
[30] M. Srivastava, S. Chaubey, A.K. Ojha, Mater. Chem. Phys. 118 (2009) 174–180.
[31] Y. Ahn, E.J. Choi, S. Kim, H.N. Ok, Mater. Lett. 50 (2001) 47–52.
[32] H.M. Zaki, S.F. Mansour, J. Phys. Chem. Solids 67 (2006) 1643–1648.
[33] S. Balaji, R. Kalai Selvan, L. John Berchmans, S. Angappan, K. Subramanian, C.O. Augustin, Mater. Sci. Eng. B 119 (2005) 119–124.
[34] B.D. Cullity, Introduction to Magnetic Materials, Addison-Wesley, Publishing Co. Inc., Reading, MA, 1972.
[35] S. Chikazumi, Physics of Magnetism, Wiley, New York, 1959.
[36] M. Georgea, A. Mary John, S.S. Naira, P.A. Joy, M.R. Anantharaman, J. Magn. Magn. Mater. 302 (2006) 190–195.
[37] J. Wang, Mater. Sci. Eng. B 127 (2006) 81–84.

[38] K.V.P.M. Shafi, Y. Koltypin, A. Gedanken, R. Prozorov, J. Balogh, J. Lendvai, I. Felner, J. Phys. Chem. B 101 (1997) 6409–6414.
[39] S. Seraphin, C. Beeli, J.M. Bonard, J. Jiao, P.A. Stadelmann, A. Chaltelain, J. Mater. Res. 14 (1999) 2861–2870.
[40] J.-H. Liu, L.-F. Zhang, G.-F. Tian, J.-C. Li, F.-S. Li, Acta Phys. Sin. 56 (2007) 6050–6055.
[41] Q. Liu, H. Huang, L. Lai, J. Sun, T. Shang, Q. Zhou, Z. Xu, J. Mater. Sci. 44 (2009) 1187–1191.
[42] N. Kasapoglu, A. Baykal, M.S. Toprak, Y. Koseoglu, H. Barakdar, Turk. J. Chem. 31 (2007) 659–666.
[43] S.S. Umare, R.S. Ningthoujam, S.J. Sharma, S. Shrivastava, S. Kurain, N.S. Gajbhiye, Hyperfine Interact. 184 (2008) 235–243.
[44] M.M. Rashad, O.A. Fouad, Mater. Chem. Phys. 94 (2005) 365–370.
[45] A.S. Fawzi, A.D. Sheikh, V.L. Mathe, Physica B 405 (2010) 340–344.